JOURNAL OF VIROLOGY, Dec. 2005, p. 14909–14922 Vol. 79, No. 23
0022-538X/05/$08.00+0 doi:10.1128/JVI.79.23.14909–14922.2005

Severe Acute Respiratory Syndrome Coronavirus Group-Specific Open Reading Frames Encode Nonessential Functions for Replication in Cell Cultures and Mice

Boyd Yount,[1] Rhonda S. Roberts,[1] Amy C. Sims,[1] Damon Deming,[2] Matthew B. Frieman,[1] Jennifer Sparks,[4] Mark R. Denison,[4] Nancy Davis,[3] and Ralph S. Baric[1,2,3]*

Department of Epidemiology, School of Public Health, University of North Carolina at Chapel Hill, Chapel Hill, North Carolina 27599-7435,[1] Department of Microbiology and Immunology, School of Medicine, University of North Carolina at Chapel Hill, Chapel Hill, North Carolina 27599-7290,[2] Carolina Vaccine Institute, School of Medicine, University of North Carolina at Chapel Hill, Chapel Hill, North Carolina 27599-7290,[3] and Department of Microbiology and Immunology and Department of Pediatrics, Vanderbilt University, Nashville, Tennessee[4]

Received 10 July 2005/Accepted 1 September 2005

SARS coronavirus (SARS-CoV) encodes several unique group-specific open reading frames (ORFs) relative to other known coronaviruses. To determine the significance of the SARS-CoV group-specific ORFs in virus replication in vitro and in mice, we systematically deleted five of the eight group-specific ORFs, ORF3a, OF3b, ORF6, ORF7a, and ORF7b, and characterized recombinant virus replication and gene expression in vitro. Deletion of the group-specific ORFs of SARS-CoV, either alone or in various combinations, did not dramatically influence replication efficiency in cell culture or in the levels of viral RNA synthesis. The greatest reduction in virus growth was noted following ORF3a deletion. SARS-CoV spike (S) glycoprotein does not encode a rough endoplasmic reticulum (rER)/Golgi retention signal, and it has been suggested that ORF3a interacts with and targets S glycoprotein retention in the rER/Golgi apparatus. Deletion of ORF3a did not alter subcellular localization of the S glycoprotein from distinct punctuate localization in the rER/Golgi apparatus. These data suggest that ORF3a plays little role in the targeting of S localization in the rER/Golgi apparatus. In addition, insertion of the 29-bp deletion fusing ORF8a/b into the single ORF8, noted in early-stage SARS-CoV human and civet cat isolates, had little if any impact on in vitro growth or RNA synthesis. All recombinant viruses replicated to wild-type levels in the murine model, suggesting that either the group-specific ORFs play little role in in vivo replication efficiency or that the mouse model is not of sufficient quality for discerning the role of the group-specific ORFs in disease origin and development.

Coronavirus infections are associated with severe diseases of the lower respiratory and gastrointestinal tract in humans and animals, yet little is known about the underlying molecular mechanisms governing virulence and pathogenesis. Among the human coronaviruses, severe acute respiratory disease coronavirus (SARS-CoV) infection is an attractive model to study the molecular basis for pathogenesis, given its robust in vitro growth characteristics, reverse genetics, animal models, wealth of clinical data, and several solved replicase and group-specific protein structures (15, 20, 31, 34, 36, 37, 40, 46, 47, 57, 69). SARS-CoV infection results in severe acute respiratory disease, pneumonia, and in about 10% of the cases, death (14, 31). With over 8,000 probable cases and ~774 deaths reported worldwide before intervention strategies contained the further spread of this pathogen, mortality rates exceeded 50% in elderly populations. Survivors display long-term lung and cardiac complications (24, 44). In comparison to other known human coronaviruses, SARS-CoV infection is highly pathogenic and the genetic factors responsible for the increased virulence of the SARS-CoV are not known. Obviously, identifying alleles that influence pathogenic outcomes provides a rational approach for the development of attenuated SARS-CoV strains, either for use in laboratory settings or as seed stocks for live- or killed-virus vaccines.

Human coronaviruses, members of the *Nidovirus* order, have been divided into several genogroups (7). The group I coronaviruses include human coronavirus 229E (HCV-229E), which is typically associated with the common cold. A second group I coronavirus, HCV-NL63, causes more severe lower respiratory tract disease in infants, children, and adults, worldwide (18, 64), and may also be associated with Kawasaki disease (16). The group II human coronaviruses include HCV-OC43, which has typically been associated with common colds in winter and occasional lower respiratory tract infections in children and adults, and the recently described HKU1, which was identified in two adults with pneumonia (68). However, the overall epidemiology and severity of HKU1 infection in humans remains undefined. Phylogenetic analyses have suggested that SARS-CoV either represents the prototype group IV coronavirus or can be classified as an early split-off of group II (36, 48, 54). SARS-CoV-like viruses have been isolated from civet cats, raccoon dogs, and pigs, but the civet cat is a likely reservoir (22). Molecular evolutionary studies on isolates obtained from different stages in the outbreak have implicated

* Corresponding author. Mailing address: Department of Epidemiology, School of Public Health, 2105D McGavran-Greenberg Hall, University of North Carolina at Chapel Hill, Chapel Hill, NC 27599-7435. Phone: (919) 966-3895. Fax: (919) 966-2089. E-mail: rbaric@email.unc.edu.

changes in open reading frame 1a (ORF1a), the spike (S) glycoprotein, and various group-specific ORFs (ORF3a and ORF8) as being associated with increased virulence, transmission, and pathogenicity during the epidemic (9). In civet cats and early-stage human isolates, ORF8 is encoded as a single contiguous ORF, while in middle/late-phase epidemic, strains contain a 29-nucleotide (nt) deletion that produces two ORFs, designated ORF8a and ORF8b (22).

The SARS-CoV virion contains a single-stranded, positive-polarity, 29,700-nucleotide-long RNA genome bound by the nucleocapsid (N) protein. The capsid is surrounded by a lipid bilayer containing at least three structural proteins, designated S, M, and E. The 180-kDa S glycoprotein interacts with an angiotensin-2-converting enzyme receptor to mediate entry into cells (70). In addition to the 23-kDa M glycoprotein, the E protein may be essential for efficient virion production (39). The SARS-CoV genome contains nine ORFs, the first of which encodes the viral replicase proteins required for subgenomic- and genome length RNA synthesis and virus replication (36, 48, 50). Based on studies with other coronaviruses, it is likely that SARS-CoV uses transcription attenuation to synthesize both full-length and subgenomic-length negative-strand RNAs containing antileader sequences, which then function as the templates for the synthesis of like-sized mRNAs (5, 51, 52). ORFs 2 through 8 are encoded in seven subgenomic mRNAs synthesized as a nested set of 3′ coterminal molecules in which the leader RNA sequences, encoded at the 5′ end of the genome, are joined to body sequences at distinct transcription regulatory sequences which contain a highly conserved consensus sequence (CS) (54, 63, 74). The SARS-CoV CS is ACGAAC (36, 48, 54, 63, 74). The virion structural genes S, E, M, and N are encoded in mRNA transcripts 2, 4, 5, and 9, respectively, while the group-specific ORFs are encoded on mRNAs 3, 6, 7, 8, and 9. Interspaced among the SARS-CoV structural genes are group-specific genes, ORF3a/b, ORF6, ORF7a/b, ORF8a/b, and ORF9b, which are not conserved in other coronaviruses and whose functions in replication and pathogenesis are generally unknown (36, 48, 54). Among these, ORF3a localizes in rough endoplasmic reticulum (rER)/Golgi compartments, interacts with the S and M glycoproteins, and is incorporated into virions, suggesting that it may function in virion maturation and release (28). However, group-specific ORFs from other coronaviruses like mouse hepatitis virus (MHV), feline infectious peritonitis virus (FIPV), and transmissible gastroenteritis virus (TGEV) are not essential for efficient in vitro replication (12, 13, 66) but often attenuate virulence in vivo (12, 13, 23). The development of a molecular clone for the SARS-CoV provides a useful tool to study the role of the SARS-CoV group-specific ORFs in replication and pathogenesis (74).

A relevant animal disease model for SARS-CoV pathogenesis has been difficult to identify. A variety of animal models for SARS-CoV have been reported, and infection is associated with mild acute disease in the macaque, ferret, cat, BALB/c and C57BL/6 mice, and hamster with little, if any, mortality (19, 21, 37, 38, 46, 49, 56, 65). Animal models reminiscent of late-stage human diseases have not been established. In young BALB/c mice, peak virus replication occurred on day 2 with virus clearance in a week in the absence of any clinical disease or pathological lesions. Viral antigen and RNA were detected in bronchiolar epithelial cells (56). With a molecular cDNA clone of the SARS-CoV genome, we systematically deleted several of the group-specific ORFs of the SARS-CoV genome and engineered recombinant viruses encoding a full-length ORF8. Here, we describe the replication kinetics and phenotype of these mutants in vitro and in BALB/c mice. Our data indicate that the SARS-CoV group-specific ORF3a, ORF3b, ORF6, ORF7a, and ORF7a/b can be deleted singly or in combination and that ORF8a and ORF8b can be joined into a full-length ORF8 with minimal impact on the kinetics of virus replication in vitro and in vivo. The development of a more relevant animal model for discerning the role of the group-specific ORFs in virulence and pathogenesis is likely needed.

MATERIALS AND METHODS

Virus and cells. The Urbani and infectious clone (ic) recombinant virus ic-SARS strains of SARS-CoV (AY278741) were propagated on Vero E6 cells in Eagle's minimal essential medium supplemented with 10% fetal calf serum, kanamycin (0.25 μg/ml), and gentamicin (0.05 μg/ml) at 37°C in a humidified CO_2 incubator. For virus growth, cultures of Vero E6 cells were infected at a multiplicity of infection (MOI) of 5 for 1 h and the monolayer washed two times with 2 ml of phosphate-buffered saline (PBS) and overlaid with complete minimal essential medium. Virus samples were harvested at different times postinfection and titered by plaque assay in 60-mm^2 dishes. Plaques were visualized by neutral red staining and counted at 48 h. All virus work was performed in a biological safety cabinet in a biosafety level 3 (BSL3) laboratory containing redundant exhaust fans. Personnel were double-gloved and dressed in Tyvek suits with full hoods and face shields. Powered air-purifying respirators with high-efficiency particulate air and organic vapor filters were used to provide a positive-pressure environment within the hoods.

Construction of recombinant viruses. Software programs were used to design primer pairs for the systematic removal of the various group-specific ORFs. Briefly, to delete the N-terminal one-half of ORF3a, sense and antisense primer sets #44 (5′-TGATCCTCTGCAACCTGAGC-3′) and SARS Mu1 (5′-ATCGATGGCGCGCCCACCTGCTAAGTTCGTTTATGTGTAATGTAATTTG-3′) and primer sets #3′-X5 (5′-TTAATTAATTAATTTGTTCGTTTATTTAAAACAACA-3′) and SARS Mu2 (5′-GGCGCGCCATCGATTTAATTAAGGAAGTGCAAATCCAAGAACCC-3′) were used to amplify products flanking nucleotides 25,297 and 25,686, respectively, in the SARS-CoV genome. PCR products were digested with AarI and subcloned by TA cloning into pTOPO-PCR XL for sequencing. Amplicons containing the correct sequence were digested with Swa1 and NdeI and ligated into SwaI-NdeI-digested SARS F subclone, systematically removing nucleotides 25,297 through 25,686 and introducing a multiple cloning site at ~25,296 containing an AarI, AscI, ClaI, and PacI site. To delete ORF3a/b, the #44/Mu1 amplicon was ligated with an amplicon generated with #3′-X5 and SARS Mu3 (5′-CACCTGCTAAACGAACTTATGTACTCATTCGTTTCGG-3′). These PCR products were digested with AarI, ligated, and subcloned by TA cloning to pTOPO PCR-XL for sequencing. Amplicons were digested with SwaI and NdeI and introduced back into the SwaI-NdeI-digested SARS F subclone, systematically deleting nucleotides 25,297 through 26,142 in the SARS-CoV genome. To delete ORF6, sense and antisense primer sets #44 and SARS Mu4 (5′-CACCTGCCATGTTCGTTCTGTTGTCACTTACTGTACTAGC-3′) and SARS Mu5 (5′-CACCTGCAAAACGAACATGAAAATTATTCTCTTCCTGAC-3′) and 3′-X5 were used to amplify products flanking nucleotides 27,103 and 27,266, respectively. The PCR products were digested with AarI, ligated, and subcloned into pTOPO PCR-XL vectors for sequencing. The SwaI-NdeI fragment containing the 192-bp deletion (nucleotides 27,102 through 27,293) of ORF6 was subcloned into SARS F as described previously. To delete ORF7a/b, primer sets #47 (5′-GTGCTTGCTGTTGTCTACAG-3′) and SARS Mu6 (5′-ATCGATCACCTGCCATGTTCGTTTTATGGATAATCTAACTCCATAGGTTC-3′) and SARS Mu7 (5′-ATCGATTTAATTAAGAGCTCACTTTAATTGACTTCTATTTGTG-3′) and SARS Ng1(−) (5′-CTTTGCTCTCAAGCTGGTTC-3′) were used to generate amplicons flanking nucleotides 27,304 through 27,671 in the SARS-CoV genome. The amplicons were digested with Aar1, subcloned, and sequenced. An AvrII-cut amplicon was purified and ligated back into the SARS F cDNA clone, systematically deleting nucleotides 27,304 through 27,671 and inserting an AarI, ClaI, and PacI multiple cloning site in the SARS-CoV genome. To generate a recombinant virus encoding the 29 bp that are present in early-stage isolates (SZ16 ORF8), primer pairs #47 and Mu29(−)

(5′-NNNCACCTGCTCAGGTTGGTAACCAGTAGGACAAGGATCTTCAA GCACATGAG-3′) and Ng1(−) and Mu29(+) (5′-CACCTGCTTACCAACC TGAATGGAATATAAGGTACAACACTAGGGGTAATAC-3′) were used to amplify cDNAs spanning the 29-nt deletion in SARS-CoV ORF8, systematically introducing 29 nucleotides from the SZ16 ORF8. The two PCR fragments were digested with AarI, ligated, and cloned into TA cloning vectors. Following sequence analysis, the full-length ORF8 was inserted into the SARS F clone by using AvrII sites.

Assembly of full-length cDNAs. The SARS A through F inserts were digested, separated through 0.8% agarose gels, visualized with a Darkreader Lightbox (Claire Chemical), excised, and purified using the QIAEX II DNA purification kit. The SARS A+B, C+D, and E+F fragments were ligated overnight and the products isolated (73, 74). The SARS A+B, C+D, and E+F fragments were ligated overnight at 4°C, phenol-chloroform extracted, and precipitated in isopropyl alcohol. Full-length transcripts were generated in vitro as described by the manufacturer (mMessage mMachine; Ambion) with certain modifications. To produce full-length capped SARS N gene transcripts, 1 μg of plasmid DNA encoding the SARS N gene was PCR amplified using forward primer (5′-NNG GCCTCGATGGCCATTTAGGTGACACTATAGATGTCTGATAATGGA CCCCAATC-3′) and reverse primer (5′-NNNTTTTTTTTTTTTTTTTTTTT TTTTTATGCCTGAGTTGAATCAGCAG-3′) and the amplicons purified from gels. Full-length, polyadenylated N gene transcripts were transcribed by SP6 RNA polymerase with a 2:1 ratio of cap analog to GTP (Ambion, Austin, TX), mixed with full-length transcripts, and electroporated into cells as described in the next section.

Transfection of full-length transcripts. RNA transcripts were added to 800 μl of the Vero E6 cell suspension (8.0×10^6) in an electroporation cuvette, and four electrical pulses of 450 V at 50 μF were given with a Gene Pulser II electroporator (Bio-Rad) similar to protocols previously described by our laboratory (73, 74). The presence of full-length cDNAs and transcripts was verified by separation on agarose gels and visualization by UV light. The transfected Vero cells were seeded in a 75-cm^2 flask and incubated at 37°C for 2 days. Viruses were plaque purified in Vero E6 cells and stock grown in 75-cm^2 flasks.

PCR amplification of leader-containing transcripts and PCR genotyping. Leader-containing amplicons were obtained from wild-type, icSARS-CoV, and various recombinant-virus-infected cells using primers at the 3′ end of the genome (primer 3′−; 5′-TTTTTTTTTTTTTTTTTTTTTGTCATTCTCCTAAGA AGC-3′) for reverse transcription (RT) and a second set of primers for PCR amplification of the SARS leader RNA sequence (5′-AAAGCCAACCAACCT CGATC-3′). Leader-containing amplicons were excised from gels, subcloned into TOPOII vectors, and sequenced using appropriate primers. Genotyping of wild-type and recombinant SARS-CoV was accomplished using sets of primer pairs spanning different portions of the 3′ end of the genome. Positive-sense primers #44, #45, #46, and #50 were used to genotype viruses containing deletions in ORF3a, ORF3b, and ORF6, while primer sets #47, #48, and #51 were used to genotype recombinant viruses containing deletions in ORF7a/b and those encoding a full-length civet cat SZ16 ORF8. For PCR genotyping, antisense primers included either SARS E(−) or ORF8b(−) for initial reverse transcription and then PCR amplification of amplicons spanning the various deletion mutations in the SARS-CoV genome.

Northern blot analysis. Cultures of Vero E6 cells were inoculated with the wild-type SARS-CoV Urbani strain and various recombinant viruses at an MOI of 1.0 and incubated for 1 h at 37°C. At 12 h postinfection, intracellular RNA was isolated using RiboPure reagents as directed by the manufacturer (Ambion, Austin, TX). mRNA was isolated using Oliogtex mRNA spin column reagents according to the manufacturer's directions (QIAGEN, Valencia, CA). The mRNA was treated with glyoxal and separated on agarose gels using Northern-Max-Gly according to the manufacturer's directions (Ambion, Austin, TX). The RNA was transferred to a BrightStar-Plus membrane (Ambion) for 4 to 5 h and the RNA cross-linked to the membrane with UV light. The blot was prehybridized and probed with an N-gene-specific oligodeoxynucleotide probe (5′-CTT GACTGCCGCCTCTGCT^{b}T^{b}CCCT^{b}CT^{b}GC^b-3′), where biontinylated nucleotides are designated with a superscript b. Blots were hybridized overnight and washed with low- and high-stringency buffers as recommended by the manufacturer. Filters were incubated with streptavidin-AP, washed, and then incubated with the chemiluminescent substrate CDP-STAR. The blots were overlaid with film and developed.

Confocal and fluorescent imaging. Antiserums were prepared in mice using Venezuelan equine encephalitis (VEE) virus replicon particles (VRPs) expressing either the SARS-CoV S, N, or ORF3a proteins. Consensus sequences of the SARS S glycoprotein, N protein, and ORF3a were inserted into the pVR21 VEE replicon vector by overlapping-extension PCR using the SARS-CoV and VEE-specific primer pairs and PCR conditions previously described by our laboratory (3). VRPs encoding the SARS-CoV S glycoprotein, N protein, or ORF3a protein were produced as previously described. The VRPs were inoculated into the footpads of 4-week-old mice at 0 and 30 days postinfection (priming and booster) and serum harvested ~2 weeks postboost (25, 26). The production and characterization of guinea pig antiserum directed against the SARS-CoV replicase nsp8 protein has previously been reported (45).

For fluorescent microscopy, Vero cells were grown on glass coverslips and infected with SARS-CoV or various deletion mutants at an MOI of 5.0 PFU/cell. Cells were infected for 12 h and rinsed with PBS. The infected cells were fixed in ice-cold 100% methanol overnight, washed with PBS, and blocked in PBS containing 5% bovine serum albumin (BSA). Cells were washed with PBS containing 1% BSA, 0.05% NP-40, and 2% normal goat serum and the coverslips incubated with primary antibody diluted 1:1,000 in PBS containing 1% BSA, 0.05% NP-40, and 2% normal goat serum. Secondary antibody was fluorescein isothiocyanate-conjugated anti-mouse antibody diluted 1:1,000 in PBS containing 1% BSA, 0.05% NP-40, and 2% normal goat serum. Coverslips were washed, mounted, and visualized with a Nikon Microphot FXA Upright fluorescence microscope.

Western blot analysis. Twelve hours postinfection, Urbani, icSARS-CoV, icSARS ΔORF3a, and ΔORF6 deletion-virus-infected cells were washed in 1× PBS and lysed in buffer containing 20 mM Tris-HCl (pH 7.6), 150 mM NaCl, 0.5% deoxycholine, 1% Nonidet P-40, 0.1% sodium dodecyl sulfate (SDS), and postnuclear supernatants added to an equal volume of 5 mM EDTA and 0.9% SDS, resulting in a final SDS concentration of 0.5%. Samples were then heat inactivated for 30 min at 90°C in the BSL3 laboratory prior to removal. At the BSL2 laboratory, samples were again heat inactivated for 30 min at 90°C before use. Equivalent sample volumes were loaded onto 4 to 20% Criterion gradient gels (Bio-Rad) and transferred to a polyvinylidene difluoride membrane (Bio-Rad). Blots were probed with polyclonal mouse antisera directed against VRP-expressed ORF3a diluted 1:200 and developed using enhanced chemiluminescence reagents (Amersham Biosciences).

To determine whether convalescent human sera could detect the ORF3a protein, equal volumes of lysate from cells infected with VEE-VRP expressing ORF3a were loaded onto 4 to 20% gradient Criterion gels (Bio-Rad) and transferred to a polyvinylidene difluoride membrane (Bio-Rad). Blots were probed with convalescent human serum 1128 diluted 1:2,000 and developed using enhanced chemiluminescence reagents (Amersham Biosciences).

SARS inoculation of mice. Six-week-old female BALB/c mice (Charles River Laboratories) were anesthetized with ketamine (1.3 mg/mouse) mixed with xylazine (0.38 mg/mouse) that was administered by intraperitoneal injection in a 50-μl volume. Each mouse was intranasally inoculated with 50 μl of PBS containing virus at a concentration of 2×10^5 PFU/ml of virus. Five animals were used for each test virus. At two days, the right lung was removed and frozen at −70°C for later determination of viral titers. Half of the left lung was placed into Trizol reagent (Invitrogen) for RNA extraction. The second half of the left lung was fixed in 4% paraformaldehyde in PBS (pH 7.4) for at least 7 days prior to paraffin embedding and sectioning for histopathological analysis (56). For virus titrations, lungs were weighed and homogenized in 4 equivalent volumes of diluent [PBS with 1% FC(II), 1 mM Ca^{2+}, and 1 mM Mg^{2+}] to generate a 20% solution. The cell suspension was centrifuged at 13,000 rpm for 5 min and the clarified supernatant serially diluted in PBS, and 200-μl volumes of each dilution were placed on a monolayer of Vero cells in 60-mm dishes. Following 1-h incubation at room temperature, cells were overlaid with 1% agarose containing complete medium. Two days later, plates were stained with neutral red and the plaques visualized and counted.

Six-week-old female BALB/c mice were also inoculated with wild-type Urbani or icSARS-CoV SZ16 ORF8 as previously described. Groups of four animals were sacrificed on days 2, 4, and 7 as described earlier to determine if the incorporation of a full-length ORF8 was associated with increased pathogenesis or persistence. As described earlier, lungs were weighed and homogenized in four volumes of diluent and titered by plaque assays as previously described.

RESULTS

Isolation of recombinant viruses. The SARS-CoV genome has been cloned as a panel of cDNAs (SARS A through F) that can be systematically assembled into full-length cDNA from which full-length infectious transcripts can be derived. The SARS-CoV F subclone encodes the SARS group-specific ORFs. Using standard recombinant DNA approaches, we systematically deleted ORF3a (icSARS ORF3a), ORF6 (icSARS

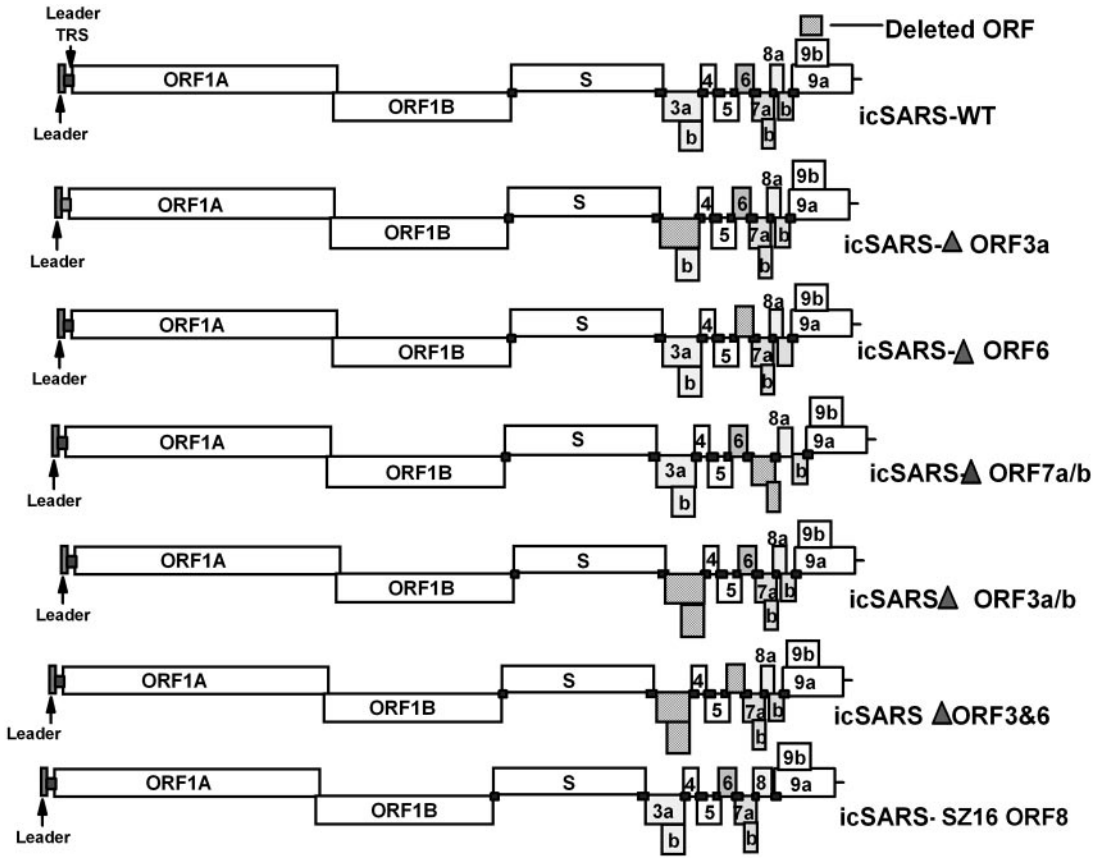

FIG. 1. Genome organization of SARS-CoV recombinant viruses. The typical genome organization of the SARS-CoV includes a ~21-kb replicase encoded in ORF1a and ORF1b; the structural genes S (ORF2), E (ORF4), M (ORF5), and N (ORF9); and the group-specific ORFs 3a (X1), 3b (X2), 6(X3), 7a(X4)/b, 8a/b(X5), and 9b. Among SARS-CoV isolates obtained from animals or early-phase human cases, ORF8a/b is fused into a single contiguous ORF8 by the presence of 29 nucleotides that are deleted in middle/late-phase epidemic strains like Urbani and Tor-2. As described in the Materials and Methods, various SARS-CoV group-specific ORFs were deleted, either individually or in combinations. The icSARS-CoV ΔORF3a lacks ORF3a, icSARS-CoV ΔORF6 lacks ORF6, and icSARS-CoV ΔORF7a/b lacks ORF7a/b, while icSARS-CoV ΔORF3a/b and icSARS-CoV ΔORF3&6 lack ORF3a/b and ORF3a/b/ORF6, respectively. The recombinant virus icSARS-CoV SZ16 ORF8 contains a full-length ORF8, produced by the insertion of the 29 nt that are present in animal and early-phase human cases that fuses ORF8a and -8b into a single ORF. Recombinant cDNAs containing the group-specific ORF deletions or insertions were confirmed by sequence analysis and used to assemble full-length cDNAs for the recovery of recombinant SARS-CoV. TRS, transcription regulatory sequence.

ORF6), and ORF7a/b (icSARS ORF7a/b) using PCR and primer pairs encoding an AarI class IIS restriction endonuclease site that allows for the seamless ligation of fragments flanking a region targeted for deletion (74). A third set of mutants lacking both ORF3a/b (icSARS ΔORF3a/b) and ORF3a/b and ORF 6 (icSARS ΔORF3&6) was also constructed. Genome organization of the mutants is shown in Fig. 1. SARS-CoV F subclones encoding the various deletions were confirmed by sequencing. The inserts were isolated after digestion with restriction endonucleases BglI and Not1 and ligated to the SARS-CoV A through E inserts. The full-length cDNA was used as template for in vitro transcription and the RNA electroporated into Vero cells for the recovery of recombinant viruses.

In vitro growth characteristics. Cultures of Vero cells were transfected with full-length transcripts lacking ORF3a, ORF6, or ORF7a/b or the various combination mutations (icSARS ΔORF3a/b, icSARS ΔORF3&6). Within 24 to 36 h posttransfection, all transfected cultures displayed clear evidence of SARS-associated cytopathology, cell rounding, and death. Supernatants were harvested and passaged onto fresh cultures, resulting in extensive cytopathology, cell rounding, and death within 36 h postinfection. Plaque purified stocks were obtained, and RT-PCR was used to demonstrate that each recombinant virus contained the appropriate genotype (Fig. 2A and B). PCR products were subcloned and sequenced, providing further verification of each particular deletion or insertion in the recombinant genome (Fig. 2C). Plaque phenotype was similar among the panel of recombinant viruses and wild-type Urbani (data not shown).

Vero cells were inoculated with the panel of wild-type and recombinant viruses at an MOI of 1.0, and virus samples were harvested at various times postinfection. Consistent with reports describing other coronaviruses lacking group-specific ORFs, recombinant viruses replicated as efficiently as wild-type virus, approaching titers of 10^7 PFU/ml within 24 h postinfection. Deletion of ORF3a resulted in the greatest reduction of virus yields, about a 0.5 to 1 log reduction in Vero, MA104, and Caco2 cells (Fig. 3). Other recombinants grew as efficiently as wild-type virus. As earlier studies have implicated ORF3a as

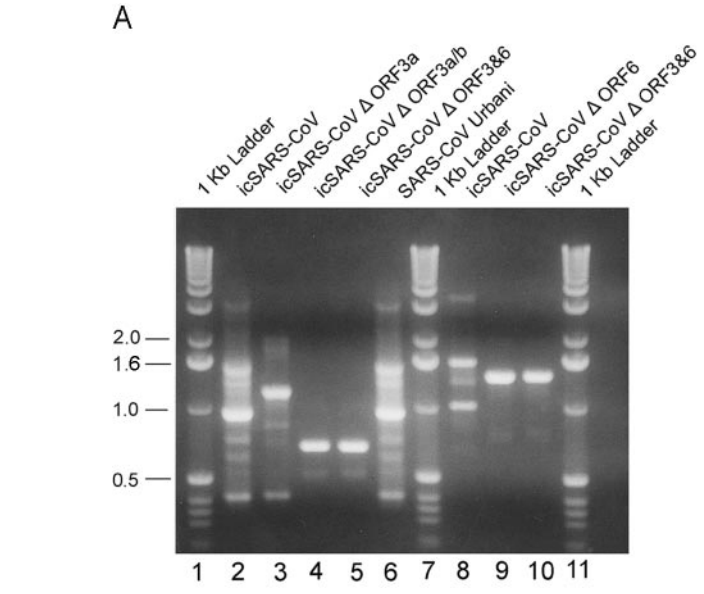

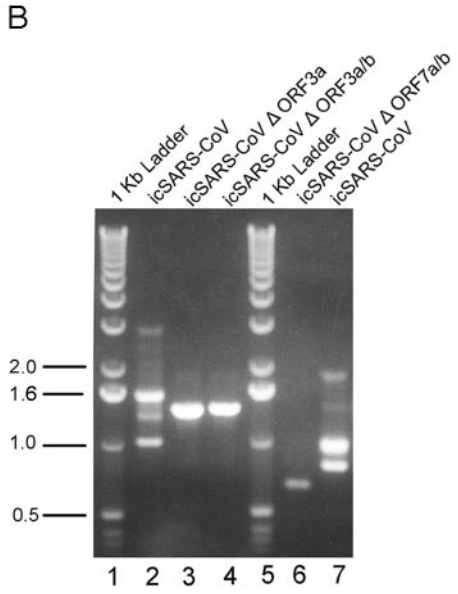

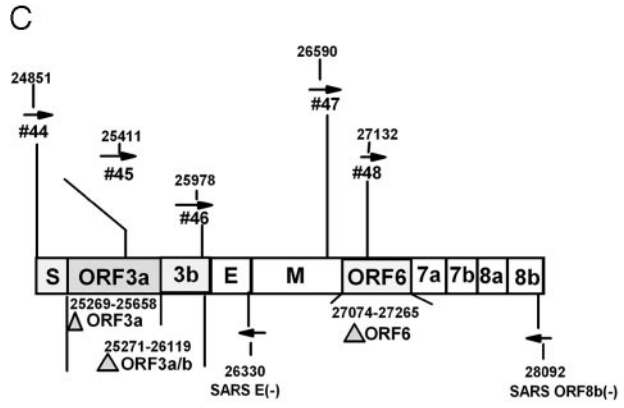

	SARS E(-)			SARS ORF8b (-)	
	44	45	46	47	48
SARS WT	1547	937	370	1528	987
Δ ORF3A	1158	-	370	1528	987
Δ ORF3A/B	699	-	-	1528	987
Δ ORF6	1547	937	370	1337	-

FIG. 2. Genotype characterization of recombinant viruses. Cultures of Vero cells were electroporated with full-length transcripts derived from different recombinant full-length cDNAs. Virus progeny were harvested between 24 and 36 h posttransfection and plaque purified and stocks generated for future studies. Cultures of cells were infected with stock viruses and intracellular RNA harvested at 12 h postinfection. Using various primer pairs that span the deletions, recombinant viruses were genotyped by RT-PCR (panels A and B). Primer location and expected sizes of PCR amplicons are shown in panel C. Primer pairs #44, #45, and #46 and SARS CoV E(−) were used in panel A, while primer pairs #47 and 48 and SARS-CoV ORF8b(−) were used in panel B. These data confirm that the deletions inserted into the component clones were found in the appropriate recombinant viruses. WT, wild type.

a structural protein (28), these results suggest that ORF3a is not absolutely required for particle formation but may reduce the efficiency of packaging and release. Alternatively, overexpression of ORF3b may also mitigate a deleterious phenotype in the icSARS-CoV ΔORF3a mutant. Consistent with this interpretation, deletion of ORF3a/b resulted in increased virus titers when compared with the ORF3a deletion virus alone, suggesting that the reduction in icSARS-CoV ORF3a virus yields might be associated with increased ORF3b expression resulting from the movement of ORF3b to the 5′ end of mRNA 3 (Fig. 3). The most debilitated virus, however, had deletions excising ORF3a/b and ORF6, which displayed about a 1 to 1.5 log reduction in titer when compared with wild-type viruses (Fig. 3). These data indicate that the group-specific ORFs 3a, 3b, 6, 7a, and 7b are not essential for replication in cell culture, similar to earlier reports regarding the roles of group-specific ORFs in the replication of other coronaviruses (12, 13, 71).

Genome organization and RNA synthesis. SARS-CoV encodes both full-length and subgenomic-length mRNAs during infection, and these RNAs are arranged in the form of a nested set from the 3′ end of the genome. Consequently, deletions of various ORFs are expected to cause a reduction in the size of all subgenomic transcripts that are upstream of the deletion. To assess the impact of group-specific ORF deletion on SARS-CoV RNA synthesis, cultures of Vero cells were inoculated with various recombinant or wild-type viruses and intracellular RNA harvested for Northern blot analysis (Fig. 4). Using a probe specific for the nucleocapsid gene, wild-type- and icSARS-CoV-infected cultures expressed both full-length RNAs and the expected eight subgenomic mRNAs. Deletion virus transcripts were characterized by the loss of specific transcripts encoding the particular ORF deleted from each recombinant virus and typified by the reduction in the size of the larger mRNAs, like mRNA 2 encoding the S glycoprotein. As expected, viruses lacking several ORFs displayed larger-size reductions in mRNA 2, as well as the loss of specific mRNAs encoding the deleted ORF in each recombinant virus. Consistent with earlier reports with MHV group-specific deletion mutants, we have not seen a major alteration in the relative

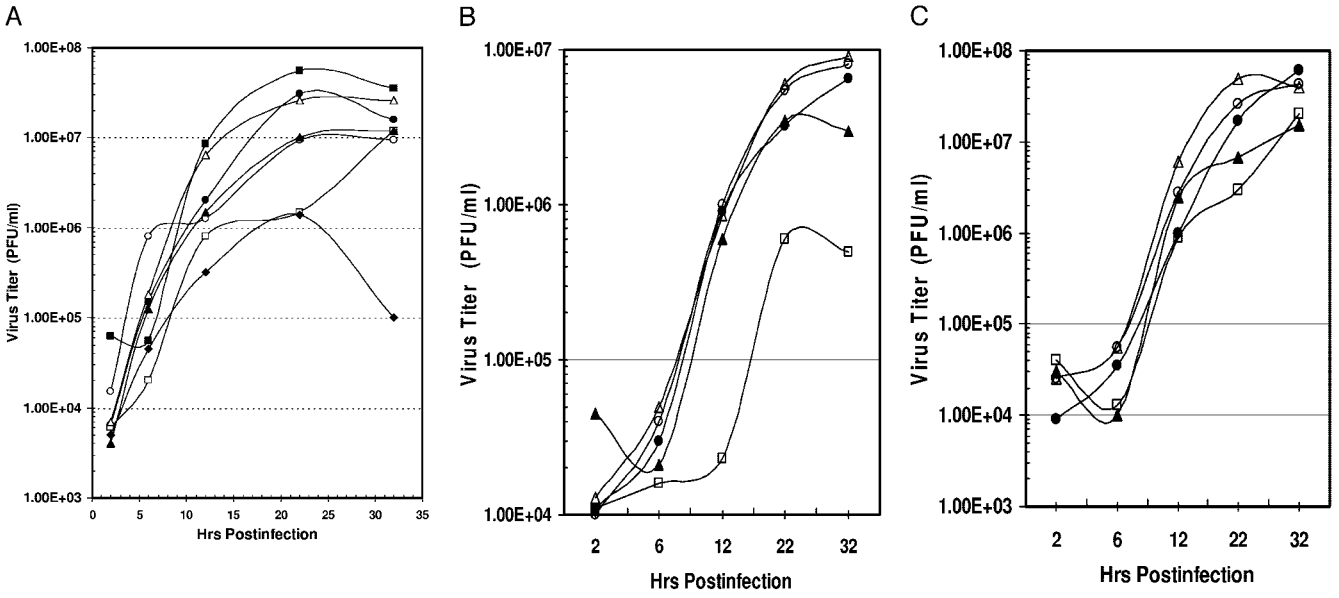

FIG. 3. Recombinant virus growth kinetics. Cultures of Vero, MA104, or human CACO2 cells were inoculated with various recombinant or wild-type viruses at an MOI of 1.0. Samples were taken at the indicated times and virus titers determined by plaque assay in Vero cells. (A) Growth in Vero cells; (B) growth in MA104 cells; (C) growth in CACO2 cells. Symbols: ●, Urbani SARS-CoV; ○, icSARS-CoV; □, icSARS-CoV ΔORF3a; ■, icSARS-CoV ΔORF3; △, icSARS-CoV ΔORF6; ▲, icSARS-CoV ΔORF7; ◆, icSARS-CoV ΔORF3&6.

molar ratios of the genomic or upstream subgenomic mRNAs following deletion.

We also examined the sites of leader/body mRNA fusion in the recombinant viruses. In each case, subgenomic mRNAs initiated at the appropriate upstream CS site, even in those recombinant viruses that had deleted ORFs, consistent with the notion that a functional transcriptional regulatory sequence consisted primarily of upstream and consensus sequences with minor contributions of downstream sites (data not shown).

A VEE replicon particle (VRP-ORF3a) expressing SARS ORF3a was constructed and used to infect Vero cells as described in the Materials and Methods. Using the convalescent antiserum from a human patient infected with SARS-CoV (#1128), expression of ORF3a from VRP-ORF3a-infected Vero cells was demonstrated, confirming earlier reports that antiserum from human patients detects ORF3a (Fig. 5A). The VRPs were then used to inoculate mice at 0 and 28 days (prime and boost), and ORF3a-specific antiserum was harvested ~2 weeks postboost. Cultures of Vero cells were infected with icSARS-CoV, wild-type Urbani SARS-CoV, icSARS-CoV ΔORF3a, and icSARS-CoV ΔORF6, and proteins were isolated for Western blot analysis at 12 h postinfection. Proteins were separated on polyacrylamide gels and probed with antiserum raised against ORF3a. As expected, ORF3a was clearly evident as a predominant ~30-kDa glycoprotein in Urbani SARS-CoV, icSARS-CoV, and icSARS-CoV ΔORF6 deletion-virus-infected cultures but was missing from mock-infected cultures or cultures infected with icSARS-CoV ΔORF3a (Fig. 5B). Similar results were noted with the icSARS-CoV ORF3a/b and the icSARS-CoV ORF3&6 deletion mutants. We did not see any major differences in the levels of S glycoprotein or N protein expression (data not shown). The murine ORF3a antiserum did not neutralize Urbani or icSARS-CoV infectivity at a 1:50 or greater concentration. Together, these data demonstrate that several of the accessories' ORFs of SARS-CoV are not essential for in vitro replication.

Colocalization with S and replicase proteins. Although detailed functional studies of each of the group-specific ORFs are still ongoing, the recovery of viable viruses suggests that these proteins do not play critical roles in regulating SARS-CoV transcription and replication or in targeting the S glycoprotein to particular membrane compartments essential for assembly and release. To test this hypothesis more thoroughly, we examined the intracellular distribution of the ORF3a protein relative to the S glycoprotein and tested whether its deletion altered S glycoprotein localization in cell membranes. Cultures of cells were infected with wild-type Urbani SARS-CoV and fixed as described in the Materials and Methods at 6, 9, or 12 h postinfection. Using antiserum directed against the nsp8 (p22) replicase protein that is known to be associated with SARS-CoV replication complexes (45) and murine antiserum directed against the SARS-CoV ORF3a, S glycoprotein, or N protein (prepared as described above for ORF3a), only the N protein colocalized with SARS-CoV replicase complexes, as evidenced by colocalization with nsp8 (p22). Neither the S glycoprotein nor ORF3a colocalized with nsp8 (p22) replicase proteins (Fig. 6). ORF3a distribution was punctuate and reticular, consistent with a rER distribution that has been reported by other groups (Fig. 6A) (28, 62). The S glycoprotein distribution was primarily Golgi apparatus and surface membrane expression, while N was tightly complexed with nsp8 (p22) as well as throughout the cytoplasm of infected cells (Fig. 6B and C, respectively).

Bioinformatic analyses and experimental studies suggest that the SARS-CoV S glycoprotein lacks an rER localization signal (53) and may require a chaperone protein for directing

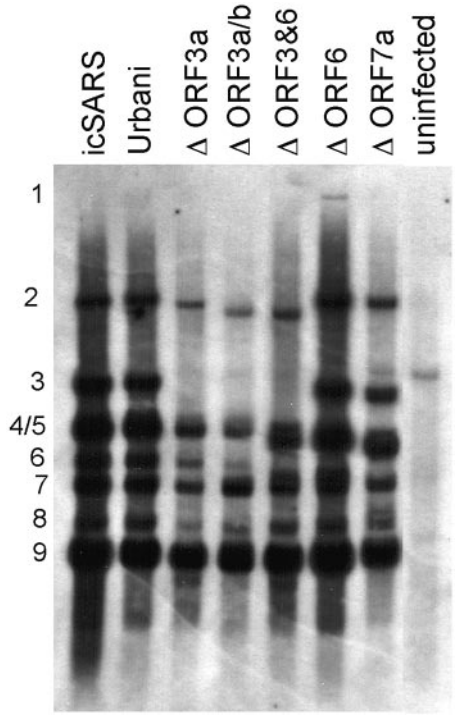

FIG. 4. Recombinant virus RNA synthesis. Cultures of Vero cells were infected with various recombinant or wild-type viruses at an MOI of 1.0. Intracellular RNA was isolated as described in the Materials and Methods and separated on 1% agarose gels. The RNA was transferred to a BrightStar-Plus membrane (Ambion) for 4 to 5 h and the RNA cross-linked to the membrane by UV light. The blot was probed with an N-gene-specific oligodeoxynucleotide probe (5′-CTTGACTGCCGC CTCTGCT^{b}T^{b}CCCT^{b}CT^{b}GC^{b}-3′), where biontinylated nucleotides are designated with a superscript b. Blots were hybridized overnight and washed with low- and high-stringency buffers as recommended by the manufacturer (BrightStar BioDetect chemiluminescent detection system; Ambion). Filters were overlaid with film and developed.

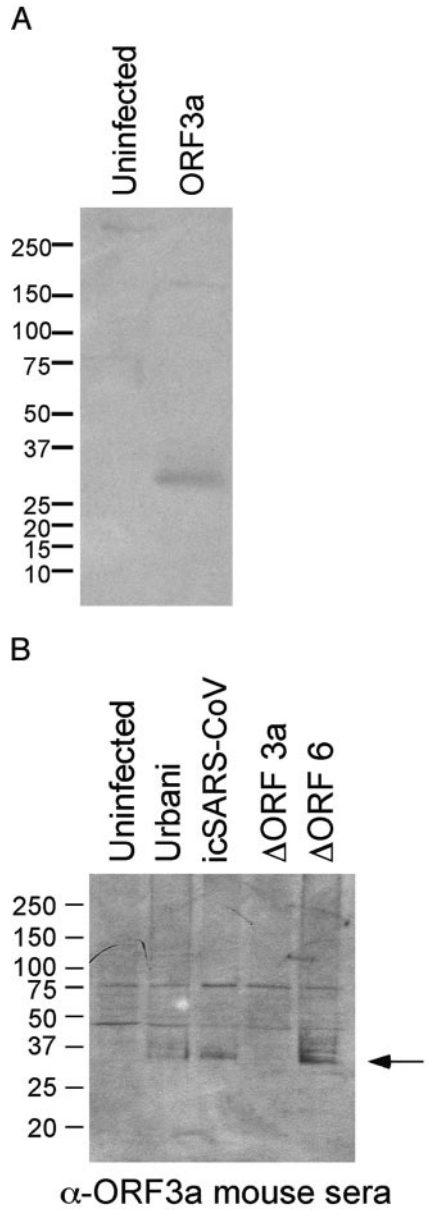

FIG. 5. Expression of ORF3a in VRP and recombinant viruses. Vero cells were infected with VRPs encoding the SARS ORF3a (VRP-ORF3a) (A) or with various recombinant or wild-type SARS-CoV (B). The proteins were harvested at 12 h postinfection, separated on polyacrylamide gels, and probed with convalescent human antiserum #1128 from a SARS-CoV-infected patient (A) or antiserum raised from mice inoculated with VRP-ORF3a (B).

localization to the SARS-CoV budding compartment. To determine if ORF3a altered S glycoprotein subcellular localization, cultures of icSARS-CoV, Urbani, or icSARS-CoV Δ3a were fixed and probed with rabbit antiserum directed against S glycoprotein or murine ORF3a antiserum. As expected, ORF3a expression is lacking from the icSARS-CoV Δ3a mutant (Fig. 7). In agreement with earlier reports, ORF3a primarily localized in rER/Golgi complexes in infected Vero cells but was also present to a lesser extent in other membranes of the cell. Although icSARS-CoV Δ3a cultures lacked ORF3a proteins, S glycoprotein localization was not markedly altered, retaining the intense punctuate staining in the Golgi apparatus/ER and surface membranes of the cell that are seen in wild-type-infected cells. This result reduces the likelihood that ORF3a chaperones S glycoprotein localization to particular intracellular membrane sites associated with virion maturation and release.

In vivo replication in mice. Deletion of one or more of the group-specific ORFs in MHV, FIPV, and TGEV results in marked reductions in virulence. To determine if the deletion of SARS-CoV group-specific ORFs altered in vivo replication, five BALB/c mice were intranasally challenged with 2×10^5 PFU of Urbani, icSARS-CoV, icSARS-CoV ΔORF3a, icSARS-CoV ΔORF3a/b, icSARS-CoV ΔORF6, icSARS-CoV ΔORF7a/b, and icSARS-CoV ΔORF3&6 recombinant viruses. At 2 days postinfection, the animals were sacrificed and virus titers/g of lung tissue determined by plaque assay (Fig. 8A). These data demonstrate that Urbani and the recombinant viruses replicated to titers of about 1×10^7 PFU/g by 2 days postinfection. The replication of icSARS ΔORF3&6 to wild-type levels in vivo differs from the noted reduction in growth seen in in vitro cultures. Mice vaccinated twice at 0 and 28 days with VRPs encoding ORF3a mounted robust immune re-

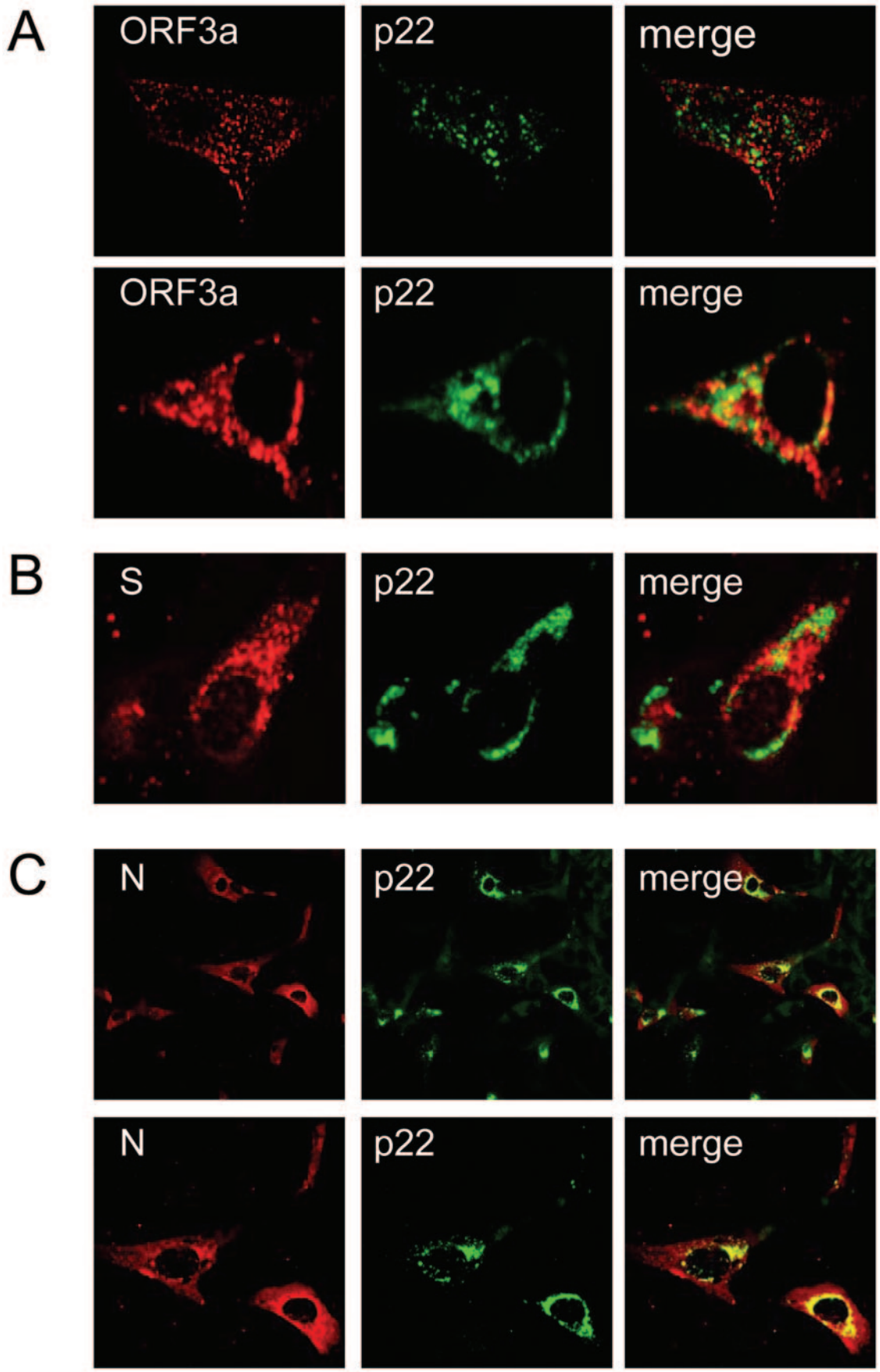

sponses that did not protect against SARS-CoV infection at 4 weeks postboost (data not shown).

It has been postulated that the 29-bp deletion in SARS-CoV Urbani ORF8 is an essential alteration for enhanced pathogenesis in humans and may function to ameliorate pathogenesis in animals (9). It is also possible that this alteration is necessary for efficient replication or persistence in animals (44). Therefore, another mutant was constructed in which the 29-bp deletion in the Urbani ORF8 gene was restored, patterned after the civet cat SZ16 ORF8 sequence as a model (icSARS-SZ16 ORF8) (Fig. 1). The icSARS-SZ16 ORF8 recombinant replicated efficiently in Vero cells and in rodents, equivalent to wild-type virus (Fig. 8B), and wild-type amounts of mRNA were detected by Northern blotting (data not shown). RT-PCR genotyping and sequence analysis confirmed the presence of the 29-bp insertion in the icSARS-SZ16 ORF8 genome (Fig. 8C). In mice at day 2 postinfection, icSARS-SZ16 ORF8 replicated to wild-type levels, approaching $\sim 1 \times 10^7$ PFU/g (Fig. 8A). No significant increases in the duration of virus persistence or replication were noted, as icSARS-CoV and icSARS-SZ16 ORF8 titers were nearly identical at similar time points postinfection (mean $6.2 \pm 1.0 \times 10^4$ on day 4) and were mostly cleared by day 7 in agreement with earlier reports in the literature with wild-type Urbani ($\sim$20% of animals had residual virus titers of low 10^2 PFU/ml) (56). These data suggest that an intact SZ16 ORF8 does not enhance the replication efficiency, duration of replication, or pathology of SARS-CoV in mice, although it is not clear whether this ORF influences pathogenesis in other animal models. Clearly, group-specific ORFs have little impact on in vivo disease in the mouse model.

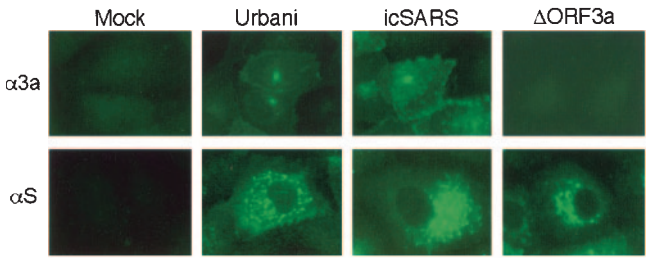

FIG. 7. Subcellular distribution of S glycoprotein in group-specific ORF deletion viruses. Cultures of Vero cells were inoculated with wild-type Urbani SARS-CoV, icSARS-CoV, or icSARS-CoV ΔORF3a. At 12 h, the infected cells were fixed in ice-cold 100% methanol overnight, washed with PBS, and blocked in PBS containing 5% BSA. Cells were washed and the coverslips incubated with mouse anti-S or ORF3a antibody diluted 1:1,000 in PBS containing 1% BSA, 0.05% NP-40, and 2% normal goat serum. Secondary antibody was fluorescein isothiocyanate-conjugated anti-mouse antibody diluted 1:1,000 in PBS containing 1% BSA, 0.05% NP-40, and 2% normal goat serum. Coverslips were washed, mounted, and visualized with a Nikon Microphot FXA Upright fluorescence microscope.

DISCUSSION

Human coronavirus pathogenesis. Coronaviruses often cause pneumoenteric infections, targeting both the respiratory and gastrointestinal tracts in humans and animals, yet little is known about the underlying molecular mechanisms governing virulence and pathogenesis, especially in the lung. Most studies have focused on the role of the coronavirus spike glycoprotein in regulating tropism and virulence, and clear evidence supports an important role for spike changes in pathogenesis, tropism, disease severity, protection from infection, and cross-species transmission (6, 35, 70). As extensive molecular evolution was noted in the genome after emergence and spread in human populations, SARS-CoV cross-species transmission, virulence, and pathogenesis are likely complex and multigenic traits (9). Consequently, SARS-CoV represents an excellent model for studying the underlying molecular mechanisms governing human coronavirus cross-species transmission, pathogenesis, and virulence. SARS-CoV replicates preferentially in the lung, produces severe lower respiratory tract disease, and replicates efficiently in vitro and in a variety of animal models. These findings, coupled with the availability of a molecular clone, provide the necessary infrastructure to elucidate the genetic basis for the underlying mechanisms of human coronavirus pneumotropism and pathology. Importantly, the SARS-CoV genome also encodes the largest and most complex set of group-specific ORFs of any known human coronavirus, likely encoding a rich set of functions that may modulate replication and pathogenic outcomes.

Among the *Coronaviridae*, the exact function of the group-specific ORFs is unknown. Recombinant MHV, FIPV, and TGEV lacking one or more group-specific ORFs replicate efficiently but are attenuated in vivo (12, 13, 71). Deletion of ORF5a in infectious bronchitis virus also minimally impacts in vitro growth, although in vivo phenotypes have not been reported (71). Among the closely related arteriviruses, deletion of group-specific ORFs as well as several of the minor structural proteins also minimally impacts in vitro growth (67). Products of the group-specific ORFs might disrupt or evade host innate immune responses, encode pro- or antiapoptotic activities, or impact other signaling pathways that might influence disease outcomes, as has been shown with other highly pathogenic viruses (1). Alternatively, the deletion of specific ORFs might subtly alter the overall ratios of the upstream subgenomic mRNAs, as the transcription attenuation model predicts that the expression of 3′-proximal mRNAs influences the level of upstream transcripts (51).

FIG. 6. Colocalization of SARS-CoV spike, ORF3a, and nucleocapsid proteins with replicase protein. Cultures of Vero cells were inoculated with wild-type Urbani SARS-CoV and fixed at 6 and 9 h postinfection as described in the Materials and Methods. Antisera against the SARS-CoV S glycoprotein, nucleocapsid, and ORF3a protein were used to determine cell distributions in combination with the SARS-CoV replicase protein, p22, by confocal microscopy as previously described (45). (A) Colocalization and distribution of the SARS-CoV ORF3a and p22 replicase protein at 6 h postinfection. (B) Colocalization and distribution of the SARS-CoV S glycoprotein and p22 replicase protein at 6 h postinfection. (C) Colocalization and distribution of the SARS-CoV nucleocapsid protein and p22 replicase protein at 6 h (top row) and 9 h (bottom row) postinfection.

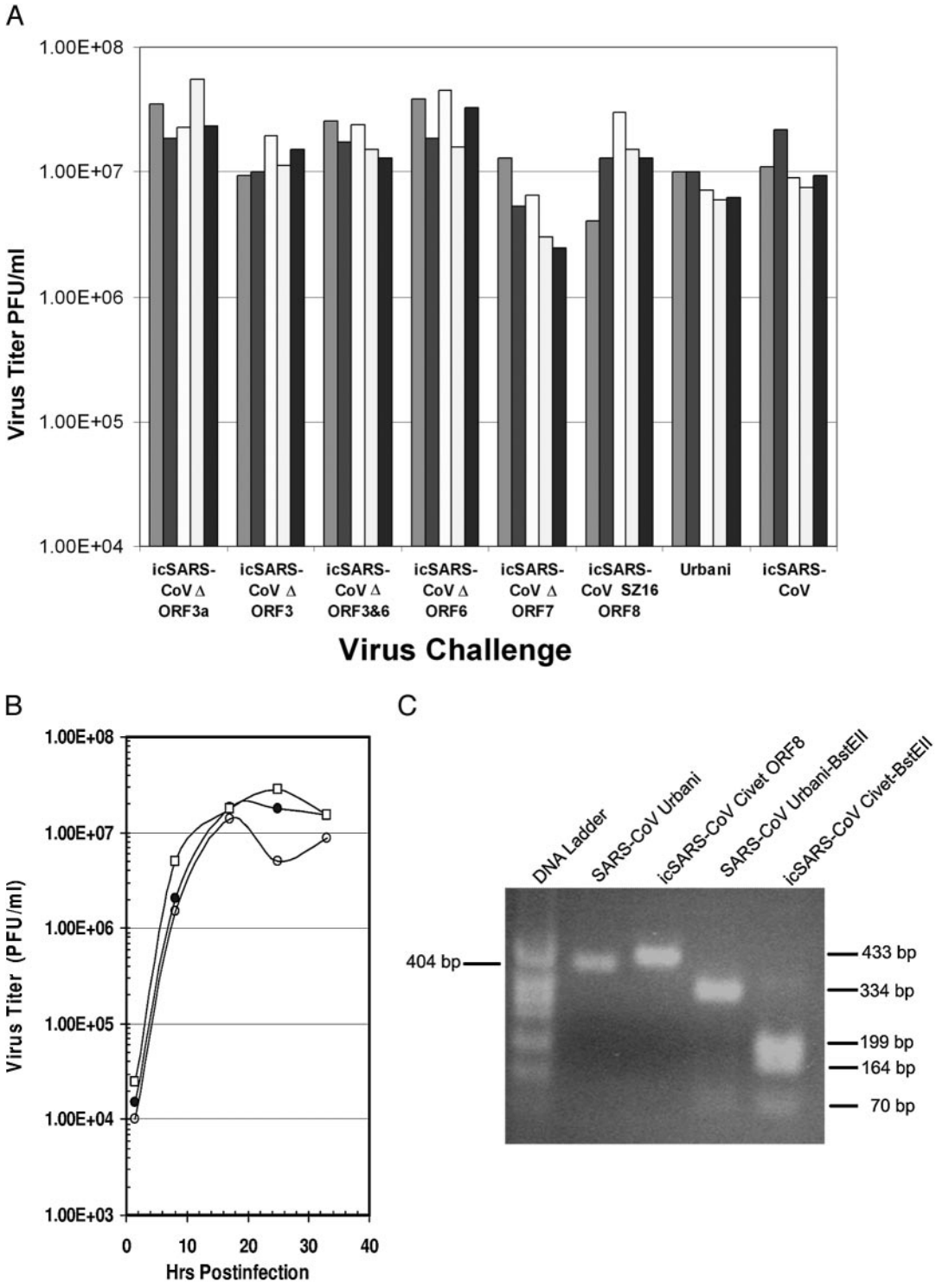

FIG. 8. In vivo replication of recombinant SARS-CoV. Six-week-old BALB/c mice were inoculated intranasally with 50 μl inoculate containing 2×10^5 PFU of wild-type and various recombinant viruses. At 2 days postinfection, the animals were sacrificed and virus titers in the lungs determined by plaque assay (A). To determine if an intact ORF8 alters in vivo pathogenesis in the murine model, a recombinant virus was constructed which included the 29 bp that fuse ORF8a/b into a single contiguous ORF. The recombinant icSARS-CoV civet SZ16 ORF8 virus replicated as efficiently as wild-type virus in Vero cells (B), contained the appropriate 29-bp insertion by RT-PCR genotyping (C), and replicated to similar titers as wild-type virus in BALB/c mice (A). Symbols: ●, Urbani SARS-CoV; ○, icSARS-CoV; □, icSARS-CoV SZ16 ORF8.

Group-specific ORF function and the murine model. In SARS-CoV, ORF3a is a structural protein that directly interacts with S and is primarily localized in the rER/Golgi apparatus. ORF3a reportedly induces apoptosis following transfection and expression in cells (28, 75). It has been reported that ORF7a is also localized in the rER/Golgi apparatus and encodes a proapoptotic activity that induces apoptosis via a caspase-dependent pathway (60). The function of ORF6 is unknown. Based on the extensive sequence analysis of SARS-CoV isolates from the wild-type and from human patients, ORF8 has been implicated in the in vivo replication of zoonotic SARS-CoV isolates as a 29-nucleotide deletion rapidly evolved following transmission into human hosts. However, the function of ORF8 and ORF8a/b in SARS-CoV infection has not been established, nor have ORF8 protein products been detected in cells.

The data from this study demonstrate that icSARS-CoV recapitulated the wild-type Urbani strain replication phenotype in the murine model and in cell cultures. Similar results were obtained with the MHV molecular clone, demonstrating that systematic assembly of full-length cDNAs results in the recovery of wild-type viruses that display similar in vitro and in vivo phenotypes (55, 73, 74). Our data also demonstrate that several SARS-CoV group-specific ORFs are nonessential for in vitro and in vivo replication. SARS-CoV infection in the murine model is not associated with clinical disease or pathology and is only an in vivo replication model. Although in humans, viral load correlates with more severe SARS-CoV disease outcomes and death (10, 27), it is unlikely that peak virus loads or duration of viral load in the murine model can be correlated with possible human infection outcomes or potential virus virulence. In humans, 10-fold or greater changes in the viral load and the duration of the viral load dramatically influence disease outcomes (10, 27), yet in many patients, peak pathology and clinical disease occur after the peak virus titer, suggesting that immune responses contribute to overall pathology and disease outcomes. Recombinant viruses lacking various group-specific ORFs displayed only ~2- to 4-fold differences in titer, indicating that these ORFs did not significantly influence in vivo replication rates in mice sufficiently to conclude evidence of an attenuated phenotype. In some cell lines, however, a few mutants displayed a ~10-fold reduction in titer, suggesting an attenuated phenotype, but more detailed analyses are needed. Although the ORF8 29-nt deletion event was correlated with expansion of the SARS-CoV epidemic in humans (9), an intact SZ16 civet cat ORF8 did not alter in vitro or in vivo replication, persistence, or the duration of the viral load in the murine model. It is possible that more dramatic ORF8 functions would be evident in civet cats or raccoon dogs, natural reservoirs for SARS-CoV replication. More robust animal models will likely be needed to dissect the genetic determinants of SARS-CoV virulence or pathogenesis in humans. SARS-CoV has also been demonstrated to replicate efficiently and produce clinical disease in hamsters and ferrets. Disease severity is more controversial in macaques, as different groups have reported varying levels of clinical disease (19, 37, 46). It is possible that one or more of these models may be necessary to unravel the function of these alleles in SARS-CoV virulence and pathogenesis. Alternatively, SARS-CoV group-specific ORFs may function in auxiliary roles that have little impact on disease outcomes or replication in vivo. Such findings would not be unprecedented, as deletion of ORF4 of MHV had little impact on in vitro replication and in vivo pathogenesis (41). However, this possibility seems less plausible given recent findings that the SARS group-specific ORF6 enhances the virulence of an attenuated murine coronavirus (42). Until these recombinant viruses can be evaluated in other models, it is prudent to consider the SARS-CoV group-specific ORF deletion viruses potentially highly pathogenic and capable of producing equivalent levels of disease in human hosts as wild-type viruses.

Group-specific ORF function in in vitro replication. ORF3a, which has an rER/Golgi localization signal, is localized to the perinuclear region of the cell and colocalized with ER and intermediate compartment markers following virus infection (62, 75). The ORF3a protein likely exists in both glycosylated and nonglycosylated forms and is incorporated into virions (28). The product of ORF3a is highly immunogenic, as indicated by the fact that antiserum from patients infected with SARS-CoV or mice inoculated with VEE replicons encoding ORF3a readily detect ORF3a by FA and Western blot analysis. The murine ORF3a antiserum ($PRNT_{50}$ [plaque reduction neutralization titer] < 50; human serum #1128 $PRNT_{50} >$ 1:1,600) did not neutralize SARS-CoV infectivity, suggesting that ORF3a does not contribute to the neutralizing antibody elicited during infection. However, we did not test whether the addition of complement enhanced ORF3a-neutralizing titers. As ORF3a-deleted viruses replicated nearly as efficiently as wild-type virus, it is likely that ORF3a is not essential for virion formation, maturation, or release. This is not the first report of a nonessential virion protein among the *Coronaviridae*. The I protein of MHV, encoded internal to the nucleocapsid gene, is also a structural protein that is not essential for virion formation; rather, viruses lacking the I ORF replicate more efficiently than wild-type virus and produce similar disease in vivo (17). The E protein of MHV, but not TGEV, is not essential for maturation and release, although replication of MHV mutants lacking the E ORF is greatly diminished compared with wild-type virus (12, 32). During assembly of the *Nidovirus* equine arteritis virus, the virion glycoproteins GP(2b), GP(3), and GP(4) form a heterotrimeric complex in the virion but are also not essential for efficient virion formation (67). Incorporation of these minor structural proteins into the virion is E protein dependent, as the absence of the E protein completely prevented the incorporation of these glycoproteins into particles.

Coronaviruses bud into the lumen of an ER-to-Golgi intermediate compartment (ERGIC) (29, 30). In virus-infected cells, the function of ORF7a remains unknown. However, its trafficking into the ER/Golgi network, the site of coronavirus budding and assembly, suggests a possible role in maturation and release (40). SARS-CoV ORF7 is divided into two ORFs designated ORF7a and -7b. Although no ORF7b product has been described to date, ORF7a encodes a 122-amino-acid type I transmembrane protein and structural studies reveal a compact seven-stranded β sandwich similar in fold and topology to members of the immunoglobulin superfamily (40). Sequences encoded in the transmembrane domain and short cytoplasmic tail mediate trafficking into the rER/Golgi apparatus. ORF7a protein can be expressed in vitro and has been detected in vivo

(8). Early studies have failed to demonstrate ORF7a in the virion; however, these studies also failed to detect E protein in virions, so additional studies are warranted (62, 75). If ORF7a is a virion protein, our data demonstrate a luxury role in virus assembly. Further support for a role of ORF7a in maturation and release are evidenced by coimmunoprecipitation studies, which indicate that ORF7a interacts with ORF3a, a protein that interacts with M, E, and S and is packaged into virions (60).

It is noteworthy that the S and ORF3a glycoproteins likely coevolved (75). ORF3a is predicted to form interchain disulfide bonds with S proteins, presumably through cysteine-rich domains localized at the junction between the putative transmembrane and cytoplasmic regions of the two proteins (75). The ORF 3a protein, which contains a tyrosine-dependent sorting signal in its cytoplasmic domain, is expressed on the cell surface and can be internalized. It has been suggested that ORF3a binds S and targets its localization to specific locations in the ER/Golgi network (61), as S lacks specific ER/Golgi retention signals (53). Deletion of ORF3a did not result in a significant redistribution of the subcellular localization of the S glycoprotein from concentrated punctuate localization in the ER/Golgi network to more diffuse or surface-staining patterns throughout the cell. Alternatively, ORF3a may interact with several proteins that in turn interact with the S glycoprotein and target its localization into sites of budding. When individually expressed, both the M glycoprotein and E protein traffic through the budding compartment, but it is not clear what makes M and E gather in the ERGIC during infection (11, 59). The M glycoprotein also specifically interacts with E and S and mediates localization of these glycoproteins into the ERGIC. At this time, it is unclear whether the subcellular localization of the SARS-CoV E and/or M glycoprotein is altered in any of the group-specific ORF deletion viruses.

Coronavirus group-specific ORFs may function to circumvent host cell innate and adaptive immune responses, as observed with a wide array of other viruses (1, 43). Not surprisingly, the deletion of group-specific ORFs attenuated many coronaviruses, although at this time, the mechanism of attenuation is not known. In SARS-CoV, it is unlikely that any of the group-specific ORFs play a critical role in the replication complex, especially in light of colocalization studies that reveal that ORF3a does not colocalize with replicase proteins that traffic into the replication complex and that deletion of ORF3b, ORF6, or ORF7a/b did not significantly alter in vitro replication phenotypes. Moreover, no significant differences in subgenomic transcription were noted among any of the deletion viruses and robust in vitro and in vivo virus growth was seen even in recombinants missing several ORFs. In contrast, the N protein interacts with the replication complex, consistent with other reports in the literature indicating a direct role of the N protein in replication and transcription processes (2, 4, 45, 72). Considering these findings and evidence suggesting a role of ORF6 in virulence (42), it seems likely that the SARS-CoV group-specific ORFs may function in modulating the intracellular environment for efficient virus replication or host responses to infection. Several viral proteins act at the plasma membrane or within the secretory pathway to alter the cell surface expression of signaling, costimulatory, and adhesion molecules or stimulate the rapid degradation of immune recognition molecules. Although ORF7a is reported to induce apoptosis and inhibit cell growth following transfection in culture, deletion of ORF7a, ORF6, or ORF3a/b did not influence cell killing, as evidenced by robust cell rounding, cytopathic effect, and death following in vitro infection (data not shown). Consequently, it seems likely that the proapoptotic characteristics of SARS-CoV infection in Vero cells are mitigated by multiple gene products. In support of this hypothesis, the N gene is capable of inducing apoptotic cell death under conditions of low serum concentration and ORF3a also may induce apoptosis and cell death (58). Moreover, some virus-host interactions are highly cell specific, further complicating the interpretation of the role of specific viral gene products in cell signaling and apoptotic cell death. Consequently, it is not surprising that the deletion of ORF7a had little overall impact on global SARS-CoV cytopathic effect, although it is possible that more subtle differences will be noted upon more detailed analyses. Construction of a recombinant virus containing an ORF3a/ORF7a deletion might display a much greater reduction in cell toxicity and death. The function of ORF3b or the presence of a specific ORF3b product in SARS-CoV-infected cells has not been reported, although deletion of ORF3 (ORF3a and ORF3b) did not result in significant reductions in virus replication or RNA synthesis, suggesting that the ORF3b gene product, if it exists, mediates functions other than RNA synthesis and in vitro replication.

SARS-CoV has renewed interest in human coronavirus pathogenesis and is a unique model for studying the molecular mechanisms governing the cross-species transmission of new coronaviruses from animal reservoirs into human populations. Among the human coronaviruses, SARS-CoV replicates efficiently in several experimental models, providing a novel environment for elucidating the genetic determinants that influence pathogenic outcomes in multiple species. In contrast, robust animal models for HCV NL63 and HCV HKU1 have not been reported, although a mouse model for HCV-229E replication and pathogenesis has been developed (33). The murine model has provided a wealth of data regarding vaccine efficacy and components of protective immunity. In this study, the in vivo replication efficiencies of the SARS-CoV group-specific ORF deletion viruses remained unchanged from the wild type in the murine model. Animal models that produce severe clinical disease/death will likely be required to unravel the critical role of the group-specific ORFs as well as other determinants of human coronavirus pathogenesis and virulence.

ACKNOWLEDGMENTS

We gratefully acknowledge technical assistance from the Carolina Vaccine Center in the preparation of this manuscript and the School of Public Health at UNC in remodeling a BSL3 facility in support of these studies. Special thanks are extended to Ande West and Martha Collier for the production of VRPs and antisera directed against SARS-CoV structural proteins.

This work was supported by the National Institutes of Health through research grants AI059136 and PO1 AI059443-01A1 to R.S.B.

REFERENCES

1. **Alcami, A., and U. Koszinowski.** 2000. Viral mechanisms of immune evasion. Immunol. Today **21:**447–455.
2. **Almazan, F., C. Galan, and L. Enjuanes.** 2004. The nucleoprotein is required for efficient coronavirus genome replication. J. Virol. **78:**12683–12688.
3. **Baric, R. S., B. Yount, L. Lindesmith, P. R. Harrington, S. R. Greene, F.-C.**

Tseng, N. Davis, R. E. Johnston, D. G. Klapper, and C. L. Moe. 2002. Expression and self-assembly of Norwalk virus capsid protein from Venezuelan equine encephalitis virus replicons. J. Virol. **76:**3023–3030.
4. **Baric, R. S., G. W. Nelson, J. O. Fleming, R. J. Deans, J. G. Keck, N. Casteel, and S. A. Stohlman.** 1988. Interactions between coronavirus nucleocapsid protein and viral RNAs: implications for viral transcription. J. Virol. **62:** 4280–4287.
5. **Baric, R. S., and B. Yount.** 2000. Subgenomic negative-strand RNA function during mouse hepatitis virus infection. J. Virol. **74:**4039–4046.
6. **Baric, R. S., B. Yount, L. Hensley, S. A. Peel, and W. Chen.** 1997. Episodic evolution mediates interspecies transfer of a murine coronavirus. J. Virol. **71:**1946–1955.
7. **Cavanagh, D.** 1997. Nidovirales: a new order comprising Coronaviridae and Arteriviridae. Arch. Virol. **142:**629–633.
8. **Chen, Y., B. Shuang, Y. Tan, M. Meng, P. Han, N. Mo, Q. Song, X. Qui, X. Luo, Q. Gan, X. Zhang, Y. Zheng, S. Liu, X. Wang, N. Zhong, and D. Ma.** 2005. The protein X4 of severe acute respiratory syndrome-associated coronavirus is expressed on both virus-infected cells and lung tissue of severe acute respiratory syndrome patients and inhibits growth of Balb/c 3T3 cell line. Chin. Med. J. (Engl. ed.) **118:**267–274.
9. **Chinese SARS Molecular Epidemiology Consortium.** 2004. Molecular evolution of the SARS coronavirus during the course of the SARS epidemic in China. Science **303:**1666–1669.
10. **Chu, C. M., L. L. M. Poon, V. C. C. Cheng, K.-S. Chan, I. F. N. Hung, M. M. L. Wong, K.-H. Chan, W.-S. Leung, B. S. F. Tang, V. L. Chan, W.-L. Ng, T.-C. Sim, P.-W. Ng, D. M. W. Tse, J. S. M. Peris, and K.-Y. Yuen.** 2004. Initial viral load and the outcomes of SARS. Can. Med. Assoc. J. **171:**1349–1352.
11. **Corse, E., and C. E. Machamer.** 2002. The cytoplasmic tail of infectious bronchitis virus E protein directs Golgi targeting. J. Virol. **76:**1273–1284.
12. **Curtis, K. M., B. Yount, and R. S. Baric.** 2002. Heterologous gene expression from transmissible gastroenteritis virus replicon particles. J. Virol. **76:**1422–1434.
13. **de Haan, C. A., P. S. Masters, X. Shen, S. Weiss, and P. J. Rottier.** 2002. The group-specific murine coronavirus genes are not essential, but their deletion, by reverse genetics, is attenuating in the natural host. Virology **296:**177–189.
14. **Drosten, C., S. Gunther, W. Preisner, S. van der Werf, H. Brodt, S. Becker, H. Rabenau, et al.** 2003. Identification of a novel coronavirus in patients with severe acute respiratory syndrome. N. Engl. J. Med. **348:**1967–1976.
15. **Egloff, M., F. Ferron, V. Campanaccii, S. Longhi, C. Rancurel, H. Dutartre, E. Snijder, A. Gorbalenya, C. Cambillau, and B. Canard.** 2004. The severe acute respiratory syndrome-coronavirus replicative protein nsp9 is a single-stranded RNA-binding subunit unique in the RNA virus world. Proc. Natl. Acad. Sci. USA **101:**3792–3796.
16. **Esper, F., E. Shapiro, C. Weibel, D. Ferguson, M. L. Landry, and J. Kahn.** 2005. Association between a novel human coronavirus and Kawasaki disease. J. Infect. Dis. **191:**499–502.
17. **Fischer, F., D. Peng, S. Hingley, S. Weiss, and P. Masters.** 1997. The internal open reading frame within the nucleocapsid gene of mouse hepatitis virus encodes a structural protein that is not essential for viral replication. J. Virol. **71:**996–1003.
18. **Fouchier, R., N. Hartwig, T. Bestebroer, B. Niemeyer, J. de Jong, J. Simon, and A. Osterhaus.** 2004. A previously undescribed coronavirus associated with respiratory disease in humans. Proc. Natl. Acad. Sci. USA **101:**6212–6216.
19. **Fouchier, R., T. Kuiken, M. Schutten, G. van Amerongen, G. van Doornum, B. van den Hoogen, M. Peiris, W. Lim, K. Stohr, and A. Osterhaus.** 2003. Aetiology: Koch's postulates fulfilled for SARS virus. Nature **423:**240.
20. **Franks, T., P. Chong, P. Chui, J. Galvin, R. Lourens, A. Reid, E. Selbs, P. Mcevoy, et al.** 2003. Lung pathology of severe acute respiratory syndrome (SARS): a study of 8 autopsy cases from Singapore. Hum. Pathol. **34:**743–748.
21. **Greenough, T., A. Carville, J. Coderre, M. Somasundaran, J. Sullivan, K. Luzuriaga, and K. Mansfield.** 2005. Pneumonitis and multi-organ system disease in common marmosets (Callithrix jacchus) infected with the severe acute respiratory syndrome-associated coronavirus. Am. J. Pathol. **167:**455–463.
22. **Guan, Y., B. J. Zheng, Y. Q. He, X. L. Liu, Z. X. Xhuang, C. L. Cheung, S. W. Luo, P. H. Li, L. J. Zhang, Y. J. Guan, K. M. Butt, K. L. Wong, K. W. Chan, W. Lim, K. F. Shortridge, K. Y. Yuen, J. S. Peiris, and L. L. Poon.** 2003. Isolation and characterization of viruses related to the SARS coronavirus from animals in southern china. Science **302:**276–278.
23. **Haijema, B., H. Volders, and P. Rottier.** 2004. Live, attenuated coronavirus vaccines through directed deletion of group-specific genes provide protection against feline infectious peritonitis. J. Virol. **78:**3863–3871.
24. **Han, Y., H. Geng, W. Feng, X. Tang, A. Ou, Y. Lao, Y. Xu, H. Lin, H. Liu, and Y. Li.** 2003. A follow-up study of 69 discharged SARS patients. J. Tradit. Chin. Med. **23:**214–217.
25. **Harrington, P. R., L. Lindesmith, B. Yount, C. L. Moe, and R. S. Baric.** 2002. Binding of Norwalk virus-like particles to ABH histo-blood group antigens is blocked by antisera from infected human volunteers or experimentally vaccinated mice. J. Virol. **76:**12335–12343.
26. **Harrington, P. R., B. Yount, R. E. Johnston, N. Davis, C. Moe, and R. S. Baric.** 2002. Systemic, mucosal, and heterotypic immune induction in mice inoculated with Venezuelan equine encephalitis replicons expressing Norwalk virus-like particles. J. Virol. **76:**730–742.
27. **Hung, I. F. N., V. C. C. Cheng, A. K. L. Wu, B. S. F. Tang, K. H. Chan, C. M. Chu, M. M. L. Wong, W. T. Hui, L. L. M. Poon, D. M. W. Tse, K. S. Chan, P. C. Y. Woo, S. K. P. Lau, J. S. M. Peiris, and K. Y. Yuen.** 2004. Viral loads in clinical specimens and SARS manifestations. Emerg. Infect. Dis. **10:**1550–1557.
28. **Ito, N., E. C. Mossel, K. Narayanan, V. L. Popov, C. Huang, T. Inoue, C. J. Peters, and S. Makino.** 2005. Severe acute respiratory syndrome coronavirus 3a protein is a viral structural protein. J. Virol. **79:**3182–3186.
29. **Klumperman, J., J. K. Locker, A. Meijer, M. C. Horzinek, H. J. Geuze, and P. J. Rottier.** 1994. Coronavirus M proteins accumulate in the Golgi complex beyond the site of virion budding. J. Virol. **68:**6523–6534.
30. **Krijnse-Locker, J., M. Ericsson, P. J. Rottier, and G. Griffiths.** 1994. Characterization of the budding compartment of mouse hepatitis virus; evidence that transport from the RER to the Golgi complex requires only one vesicular transport step. J. Cell Biol. **124:**55–70.
31. **Ksiazek, T. G., D. Erdman, C. Goldsmith, S. R. Zaki, T. Peret, S. Emery, S. Tong, C. Urgani, et al.** 2003. A novel coronavirus associated with severe acute respiratory syndrome. N. Engl. J. Med. **348:**1953–1966.
32. **Kuo, L., and P. S. Masters.** 2003. The small envelope protein E is not essential for murine coronavirus replication. J. Virol. **77:**4597–4608.
33. **Lassnig, C., C. M. Sanchez, M. Egerbacher, I. Walter, S. Majer, T. Kolbe, P. Pallares, L. Enjuanes, and M. Muller.** 2005. Development of a transgenic mouse model susceptible to human coronavirus 229E. Proc. Natl. Acad. Sci. USA **102:**8275–8280.
34. **Leung, T. F., G. W. Wong, K. L. Hon, and T. F. Fok.** 2003. Severe acute respiratory syndrome (SARS) in children: epidemiology, presentation and management. Paediatr. Respir. Rev. **4:**334–339.
35. **Li, W., C. Zhang, J. Sui, J. H. Kuhn, M. J. Moore, S. Luo, S.-K. Wong, I.-C. Huang, K. Xu, N. Vasilieva, A. Murakami, Y. He, W. A. Marasco, Y. Guan, H. Choe, and M. Farzan.** 2005. Receptor and viral determinants of SARS-coronavirus adaptation to human ACE2. EMBO J. **24:**1634–1643.
36. **Marra, M. A., S. J. M. Jones, C. R. Astell, R. A. Holt, A. Brooks-Wilson, Y. S. N. Butterfield, J. Khattra, J. K. Asano, et al.** 2003. The genome sequence of the SARS-associated coronavirus. Science **300:**1399–1404.
37. **Martina, B. E., B. L. Haagmans, T. Kuiken, R. A. Fouchier, G. F. Rimmelzwaan, G. Van Amerongen, J. S. Peiris, W. Lim, and A. D. Osterhaus.** 2003. Virology: SARS virus infection of cats and ferrets. Nature **425:**915.
38. **McAuliffe, J., L. Vogel, A. Roberts, G. Fable, S. Fisher, W. J. Whieh, E. Butler, S. Zaki, M. St. Claire, B. Murphy, and K. Subbarao.** 2004. Replication of SARS coronavirus administered into the respiratory tract of African Green, rhesus and cynomolgus monkeys. Virology **330:**8–15.
39. **Mortola, E., and P. Roy.** 2004. Efficient assembly and release of SARS coronavirus-like particles by a heterologous expression system. FEBS Lett. **576:**174–178.
40. **Nelson, C., A. Pekosz, C. Lee, M. Diamond, and D. Fremont.** 2005. Structure and intracellular targeting of the SARS-coronavirus ORF7a accessory protein. Structure **13:**75–85.
41. **Ontiveros, E., L. Kuo, P. S. Masters, and S. Perlman.** 2001. Inactivation of expression of gene 4 of mouse hepatitis virus strain JHM does not affect virulence in the murine CNS. Virology **289:**230–238.
42. **Pewe, L., H. Zhou, J. Netland, C. Tangudu, H. Olivares, L. Shi, D. Look, T. Gallagher, and S. Perlman.** 2005. A severe acute respiratory syndrome-associated coronavirus-specific protein enhances virulence of an attenuated murine coronavirus. J. Virol. **79:**11335–11342.
43. **Ploegh, H. L.** 1998. Viral strategies of immune evasion. Science **280:**248–253.
44. **Poon, L. L., Y. Guan, J. M. Nicholls, K. Y. Yuen, and J. S. M. Peiris.** 2004. The aetiology, origins and diagnosis of severe acute respiratory syndrome. Lancet Infect. Dis. **4:**663–671.
45. **Prentice, E., J. McAuliffe, X. Lu, K. Subbarao, and M. R. Denison.** 2004. Identification and characterization of severe acute respiratory syndrome coronavirus replicase proteins. J. Virol. **78:**9977–9986.
46. **Roberts, A., L. Vogel, J. Guarner, N. Hayes, B. Murphy, S. Zaki, and K. Subbarao.** 2005. Severe acute respiratory syndrome coronavirus infection of golden Syrian hamsters. J. Virol. **79:**503–511.
47. **Robertson, M., H. Igel, R. Baertsch, D. Haussler, M. Ares, and W. Scott.** 2005. The structure of a rigorously conserved RNA element within the SARS virus genome. PLoS Biol. **3:**86–94.
48. **Rota, P. A., M. S. Oberste, S. S. Monroe, W. A. Nix, R. Campagnoli, J. P. Icenogle, S. Penaranda, et al.** 2003. Characterization of a novel coronavirus associated with severe acute respiratory syndrome. Science **300:**1394–1999.
49. **Rowe, T., G. Gao, R. J. Hogan, R. G. Crystal, T. G. Voss, R. L. Grant, P. Bell, G. P. Kobinger, N. A. Wivel, and J. M. Wilson.** 2004. Macaque model for severe acute respiratory syndrome. **78:**11401–11404.
50. **Ruan, Y. J., C. L. Wei, A. L. Ee, V. B. Vega, H. Thoreau, S. T. Su, J. M. Chia, P. Ng, K. P. Chiu, L. Lim, T. Zhang, C. K. Peng, E. O. Lin, et al.** 2003. Comparative full-length genome sequence analysis of 14 SARS-CoV isolates and common mutations associated with putative origins of infection. Lancet **361:**1779–1785.

51. **Sawicki, S. G., and D. L. Sawicki.** 1990. Coronavirus transcription: subgenomic mouse hepatitis virus replicative intermediates function in RNA synthesis. J. Virol. **64:**1050–1056.
52. **Schaad, M. C., and R. S. Baric.** 1994. Genetics of mouse hepatitis virus transcription: evidence that subgenomic negative strands are functional templates. J. Virol. **68:**8169–8179.
53. **Schwegmann-Wessels, C., M. Al-Falah, D. Escors, Z. Wang, G. Zimmer, H. Deng, L. Enjuanes, H. Y. Naim, and G. Herrler.** 2004. A novel sorting signal for intracellular localization is present in the S protein of a porcine coronavirus but absent from severe acute respiratory syndrome-associated coronavirus. J. Biol. Chem. **279:**43661–43666.
54. **Snijder, E. J., P. J. Bredenbeek, J. C. Dobe, V. Thiel, J. Ziebuhr, L. L. Poon, Y. Guan, M. Rozanov, W. J. Spaan, and A. E. Gorbalenya.** 2003. Unique and conserved features of genome and proteome of SARS-CoV, an early split-off from the coronavirus group 2 lineage. J. Mol. Biol. **331:**991–1004.
55. **Sperry, S. M., L. Kazi, R. L. Graham, R. S. Baric, S. R. Weiss, and M. R. Denison.** 2005. Single-amino-acid substitutions in open reading frame (ORF) 1b-nsp14 and ORF 2a proteins of the coronavirus mouse hepatitis virus are attenuating in mice. J. Virol. **79:**3391–3400.
56. **Subbarao, K., J. McAuliffe, L. Vogel, G. Fahle, S. Fischer, K. Tatti, M. Packard, W.-J. Shieh, S. Zaki, and B. Murphy.** 2004. Prior infection and passive transfer of neutralizing antibody prevent repication of SARS coronavirus in the respiratory tract of mice. J. Virol. **78:**3572–3577.
57. **Supekar, V., C. Bruckmann, P. Ingallinella, E. Bianchi, A. Pessi, and A. Carfi.** 2004. Structure of a proteolytically resistant core from the severe acute respiratory syndrome coronavirus S2 fusion protein. Proc. Natl. Acad. Sci. USA **101:**17958–17963.
58. **Surjit, M., B. Liu, S. Jameel, V. Chow, and S. Lal.** 2004. The SARS coronavirus nucleocapsid protein induces actin reorganization and apoptosis in COS-1 cells in the absence of growth factors. Biochem. J. **383:**13–18.
59. **Swift, A. M., and C. E. Machamer.** 1991. A Golgi retention signal in a membrane-spanning domain of coronavirus E1 protein. J. Cell Biol. **115:** 19–30.
60. **Tan, Y., B. Fielding, P. Goh, S. Shen, T. Tan, S. Lim, and W. Hong.** 2004. Overexpression of 7a, a protein specifically encoded by the severe acute respiratory syndrome coronavirus induces apoptosis via a caspase-dependent pathway. J. Virol. **78:**14043–14047.
61. **Tan, Y. J.** 2005. The severe acute respiratory syndrome (SARS)-coronavirus 3a protein may function as a modulator of the trafficking properties of the spike protein. Virol. J. **2:**5.
62. **Tan, Y. J., E. Teng, S. Shen, Tan, T. H., P. Y. Goh, B. C. Feilding, E. E. Ooi, H. C. Tan, S. G. Lim, and W. Hong.** 2004. A novel severe acute respiratory syndrome coronavirus protein, U274, is transported to the cell surface and undergoes endoyctosis. J. Virol. **78:**6723–6734.
63. **Thiel, V., K. A. Ivanov, A. Putics, T. Hertzig, B. Schelle, S. Bayer, B. Weissbrich, E. J. Snijder, H. Rabenau, H. W. Doerr, A. E. Gorbalenya, and J. Zeibuhr.** 2003. Mechanisms and enzymes involved in SARS CoV genome expression. J. Gen. Virol. **84:**2305–2315.
64. **van den Hoogen, B., K. Pyre, M. Jebbink, W. Vermeulen-Oost, R. Berkhout, K. Wolthers, P. Wertheim-van Dillen, et al.** 2004. Identification of a new human coronavirus. Nat. Med. **10:**368–373.
65. **Weingarl, H., M. Czub, S. Chub, J. Neufeld, P. Marszal, J. Gren, G. Smith, et al.** 2004. Immunization with modified vaccinia virus ankara-based recombinant vaccine against severe acute respiratory syndrome is associated with enhanced hepatitis virus in ferrets. J. Virol. **78:**12672–12676.
66. **Wesley, R. D., R. D. Woods, and A. K. Cheung.** 1991. Genetic analysis of porcine respiratory coronavirus, an attenuated variant of TGEV. J. Virol. **65:**3369–3373.
67. **Wieringa, R., A. de Vries, J. van der Meulen, G. Godeke, J. Onderwater, H. van Tol, H. Koerten, A. Mommaas, E. Snijder, and P. Rottier.** 2004. Structural protein requirements in equine arteritis virus assembly. J. Virol. **78:** 13019–13027.
68. **Woo, P., S. Lau, C.-M. Chu, K.-H. Chan, H.-W. Tsoi, Y. Huang, B. Wong, R. Poon, et al.** 2005. Characterization and complete genome sequence of a novel coronavirus, coronavirus HKu1, from patients with pneumonia. J. Virol. **79:**884–895.
69. **Yang, H., M. Yang, Y. Ding, Y. Liu, Z. Lou, Z. Zhou, L. Sun, L. Mo, S. Ye, H. Pang, G. Gao, K. Anand, M. Bartlam, R. Hilgenfeld, and Z. Rao.** 2003. The crystal structure of severe acture respiratory syndrome virus main protease and its complex with an inhibitor. Proc. Natl. Acad. Sci. USA **100:** 13190–13195.
70. **Yang, Z., H. Werner, W. Kong, K. Leung, E. Traggiai, A. Lanzavecchia, and G. Nabel.** 2005. Evasion of antibody neutralization in emerging severe acute respiratory syndrome coronaviruses. Proc. Natl. Acad. Sci. USA **102:**797–801.
71. **Youn, S., J. Leibowitz, and E. Collisson.** 2005. In vitro assembled, recombinant infectious bronchitis viruses demonstrate that the 5a ORF is not essential for replication. Virology **332:**206–215.
72. **Yount, B., C. Curtis, and R. S. Baric.** 2000. A strategy for the assembly of large RNA and DNA genomes: the transmissible gastroenteritis virus model. J. Virol. **74:**10600–10611.
73. **Yount, B., M. R. Denison, S. R. Weiss, and R. S. Baric.** 2002. Systematic assembly of a full-length infectious cDNA of mouse hepatitis virus strain A59. J. Virol. **76:**11065–11078.
74. **Yount, B., K. Curtis, E. Fritz, L. Hensley, P. Jahrling, E. Prentice, M. Denison, T. Geisbert, and R. Baric.** 2003. Reverse genetics with a full length infectious cDNA of the severe acute respiratory syndrome coronavirus. Proc. Natl. Acad. Sci. USA **100:**12995–13000.
75. **Zeng, R., R. Yang, M. Shi, M. jiang, Y. Xie, H. Ruan, X. Jiang, et al.** 2004. Characterization of the 3a protein of SARS-associated coronavirus in infected Vero E6 cells and SARS patients. J. Mol. Biol. **34:**271–279.